博 士 論 文

The oral bacterium *Streptococcus mutans* promotes tumor metastasis by inducing vascular inflammation

（口腔細菌，*Streptococcus mutans* は、血管炎症を誘発し転移を促進する）

令和 5 年 3 月申請

北海道大学
大学院歯学院口腔医学専攻

Yu　Li

Received: 18 March 2022 | Revised: 25 July 2022 | Accepted: 31 July 2022

DOI: 10.1111/cas.15538

Cancer Science WILEY

ORIGINAL ARTICLE

The oral bacterium *Streptococcus mutans* promotes tumor metastasis by inducing vascular inflammation

Li Yu[1,2] | Nako Maishi[1] | Erika Akahori[1,2] | Akira Hasebe[3] | Ryo Takeda[1,2] | Aya Yanagawa Matsuda[1] | Yasuhiro Hida[4] | Jin-Min Nam[5] | Yasuhito Onodera[5] | Yoshimasa Kitagawa[2] | Kyoko Hida[1]

[1]Vascular Biology and Molecular Pathology, Faculty of Dental Medicine and Graduate School of Dental Medicine, Hokkaido University, Sapporo, Japan

[2]Oral Diagnosis and Medicine, Faculty of Dental Medicine and Graduate School of Dental Medicine, Hokkaido University, Sapporo, Japan

[3]Oral Molecular Microbiology, Faculty of Dental Medicine and Graduate School of Dental Medicine, Hokkaido University, Sapporo, Japan

[4]Cardiovascular and Thoracic Surgery, Faculty of Medicine Community Service and Welfare Network, Hokkaido University Hospital, Sapporo, Japan

[5]Global Center for Biomedical Science and Engineering (GCB), Faculty of Medicine, Hokkaido University, Sapporo, Japan

Correspondence
Kyoko Hida, Vascular Biology and Molecular Pathology, Faculty of Dental Medicine and Graduate School of Dental Medicine, Hokkaido University, Kita-13, Nishi-7, Kita-Ku, Sapporo 060-8586, Japan.
Email: khida@den.hokudai.ac.jp

Funding information
Japan Agency for Medical Research and Development, Grant/Award Number: JP18ck0106198h0003 and JP19ck0106406h0002; Japan Society for the Promotion of Science, Grant/Award Number: JP18H02891, JP18H02996 and JP18K09715; JST SPRING, Grant/Award Number: JPMJSP2119

Abstract

Recent studies have demonstrated a relationship between oral bacteria and systemic inflammation. Endothelial cells (ECs), which line blood vessels, control the opening and closing of the vascular barrier and contribute to hematogenous metastasis; however, the role of oral bacteria-induced vascular inflammation in tumor metastasis remains unclear. In this study, we examined the phenotypic changes in vascular ECs following *Streptococcus mutans* (*S. mutans*) stimulation in vitro and in vivo. The expression of molecules associated with vascular inflammation and barrier-associated adhesion was analyzed. Tumor metastasis was evaluated after intravenous injection of *S. mutans* in murine breast cancer hematogenous metastasis model. The results indicated that *S. mutans* invaded the ECs accompanied by inflammation and NF-κB activation. *S. mutans* exposure potentially disrupts endothelial integrity by decreasing vascular endothelial (VE)-cadherin expression. The migration and adhesion of tumor cells were enhanced in *S. mutans*-stimulated ECs. Furthermore, *S. mutans*-induced lung vascular inflammation promoted breast cancer cell metastasis to the lungs in vivo. The results indicate that oral bacteria promote tumor metastasis through vascular inflammation and the disruption of vascular barrier function. Improving oral hygiene in patients with cancer is of great significance in preventing postoperative pneumonia and tumor metastasis.

KEYWORDS
endothelial cells, oral bacteria, oral hygiene, tumor metastasis, vascular inflammation

Abbreviations: CFUs, Colony-forming units; ECs, Endothelial cells; ELISA, Enzyme-linked immunosorbent assay; EMT, Epithelial–mesenchymal transition; IPA, Ingenuity Pathway Analysis.

1 | INTRODUCTION

Cancer is the second leading cause of death globally.[1] Inflammation is associated with tumorigenesis as Dr. Rudolf Virchow proposed in 1863.[2] Moreover, many cancers possess the propensity to metastasize to sites of inflammation.[3–5] Hematogenous metastasis is responsible for 90% of tumor metastasis-associated mortality.[6,7] Therefore, it is necessary to identify the risk factors that promote hematogenous metastasis.

S. mutans is a Gram-positive bacterium associated with dental caries.[8] Poor oral hygiene, cancer chemotherapy, or radiotherapy-induced dryness or bleeding of the mouth may enhance *S. mutans* accumulation. *S. mutans* gains access to the bloodstream during invasive dental procedures, such as tooth extraction, periodontal surgery, or even daily oral hygiene practices to cause systemic diseases.[9,10] Of these, cardiovascular disease is the most common.[11,12] Blood vessels are composed of ECs and provide the nutrients and oxygen for tumor growth and metastasis.[13–17] Studies have indicated that *S. mutans* can invade ECs through Toll-like receptor 2 to cause inflammation.[18] Inflamed ECs result in hyperpermeability of the blood vessel[19]; however, the role of *S. mutans*-mediated vascular inflammation in the progression of hematogenous metastasis is unknown.

During the process of hematogenous metastasis, tumor cells first migrate toward the endothelium, then adhere to the endothelium, and finally extravasate across the endothelium to complete secondary seeding.[20] In this study, we focused on vascular inflammation and vascular integrity impairment in distant organs resulting from *S. mutans* exposure in vivo and in vitro. In addition, we determined the contribution of *S. mutans* to tumor metastasis using in vivo tumor metastasis models. Our findings provide clear evidence that oral bacteria actively promote tumor metastasis and highlight the importance of oral hygiene management in patients with cancer.

2 | MATERIALS AND METHODS

2.1 | Cell lines and culture conditions

The MS1 mouse islet-derived normal EC line, which was created by the transduction of a temperature-sensitive SV40 large T antigen, was obtained from the ATCC (Manassas, VA, USA). MS1 cells were cultured in DMEM (Sigma-Aldrich) supplemented with 10% heat-inactivated FBS and 1% penicillin/streptomycin antibiotic (Sigma-Aldrich). E0771 murine breast carcinoma cells were purchased from CH3 BioSystems and transfected with a lentiviral vector encoding tdtomato-Luc2, as described previously.[20] The tdtomato-Luc2-expressing E0771 cells were cultured in RPMI 1640 medium (Sigma-Aldrich) supplemented with 10 mM HEPES and 10% FBS. All cells were cultured at 37°C in a humidified atmosphere containing 5% CO_2. The absence of *Mycoplasma pulmonis* was verified by PCR.

2.2 | Oral bacterial strain and culture conditions

S. mutans was obtained from the ATCC (ATCC 25175) and cultured in brain–heart infusion (BHI) medium (BD) at 37°C under anaerobic conditions (90% N_2, 5% CO_2, 5% H_2). CFUs were measured by serial dilution and plating on Mitis Salivarius Bacitracin Agar medium (BD).

2.3 | Gram staining

MS1 cells were stimulated with *S. mutans* at an MOI of 1 in antibiotic-free DMEM. The cells were washed with PBS or 200 μl/mL penicillin/streptomycin antibiotic culture medium for 2 h. We found that 200 μl antibiotic was sufficient to kill 2×10^7 CFUs of *S. mutans* in 2 h (Figure S1). The cells were fixed with 4% paraformaldehyde (PFA) and stained with Gram stain (MUTO PURE CHEMICALS). Images were obtained using a BZX810 microscope equipped with BZ-X800 Analyzer software (KEYENCE).

2.4 | Bacteria colony formation assay

Bacteria colony formation assay was performed as previously reported,[21] with some modifications. MS1 cells were seeded at a density of 1×10^5 cells per plate and cultured overnight. The culture medium was replaced with antibiotic-free DMEM and stimulated by *S. mutans* at an MOI of 1 and incubated for the indicated time. After washing, the cells were incubated with medium containing 200 μl/mL penicillin/streptomycin to remove externally adherent *S. mutans*. The cells were then incubated with trypsin–EDTA (SIGMA, Darmstadt, Germany) and lysed with distilled water. The cell lysates were cultured on BHI agar medium for 2 days under anaerobic conditions. The CFUs of the invading *S. mutans* were counted using a multifunction colony counter (Heathrow Scientific) and imaged.

2.5 | Tumor cell migration assay

Tumor cell migration toward the *S. mutans*-stimulated ECs was assessed using transwell chambers (Corning, Life Sciences) as described previously,[20,22,23] with some modifications. Briefly, MS1 suspensions were placed into the lower compartment. After incubating for 6 h, the culture medium was replaced with antibiotic-free DMEM containing 5% FBS. The cells were stimulated with *S. mutans* at an MOI of 1 for 5 h, the culture medium was changed to fresh DMEM plus 5% FBS, followed by incubation for an additional 24 h. Tumor cell suspensions were maintained in serum-free medium for 24 h prior to the assays. They were then added to the upper compartment and allowed to migrate for 4 h. Nonmigrating tumor cells on the membrane were removed with a cotton swab,

followed by fixation with 4% PFA and staining with hematoxylin. Cells that migrated to the bottom surface were counted by microscopy.

2.6 | Adhesion assay

S. mutans at an MOI of 1 was added to stimulate the MS1 monolayer in antibiotic-free DMEM medium. The culture medium was replaced with PBS or penicillin/streptomycin-containing DMEM for 2 h to remove the external *S. mutans* after the indicated times. The culture medium was changed to DMEM containing 10% FBS and penicillin/streptomycin. Then, 1×10^3 tdtomato-Luc2-expressing E0771 tumor cells were added to the MS1 monolayer and allowed to adhere for 2 h. After removing nonadherent tumor cells, the remaining cells were fixed and stained with DAPI (Dojin Chemical) and counted under a fluorescence microscope.

2.7 | RNA isolation and quantitative real-time PCR

RNA from ECs and tissues was isolated using the Relia-Prep RNA tissue miniprep system (Promega) and the RNeasy Micro kit (Qiagen), respectively. cDNA synthesis and quantitative real-time PCR were performed, as described previously.[24] The primers used in this study are listed in Table S1.

2.8 | ELISA

Detailed descriptions of the methods are provided in Appendix S1.

2.9 | NF-κB inhibition

Detailed descriptions of the methods are provided in Appendix S1.

2.10 | Western blot analysis

After stimulation of MS1 with *S. mutans* in antibiotic-free DMEM at an MOI of 1, cells were lysed after the corresponding stimulation time, as described previously.[20] The total protein concentration was determined using a bicinchoninic acid (BCA) protein assay kit (Pierce Biotechnology). Western blot analysis was performed using antibodies specific for phospho-NF-κB p65 (Ser536) (93H1) (Cell Signaling, 3033S), NF-κB p65 (D14E12) (Cell Signaling, 8242S), ICAM-1 (BioLegend, 116101), and β-actin (13E5) (Cell Signaling, 4970), along with the corresponding horseradish peroxidase-conjugated secondary antibodies. The NF-κB and ICAM-1 levels were normalized to β-actin by scanning densitometry using ImageJ software.

2.11 | RNA sequencing (RNA-seq) and bioinformatics analysis

Detailed descriptions of the methods are provided in Appendix S1.

2.12 | Immunocytochemistry

After culturing MS1 on coverslips with *S. mutans* at an MOI of 1 in antibiotic-free DMEM, the cells were fixed in 4% PFA and stained with anti-mouse VE-cadherin antibody (BD Pharmingen) and anti-rabbit Alexa Fluor 647 secondary antibody (BioLegend, 405416) and counterstained with DAPI. Images were obtained using a fluorescence microscope and quantified using ImageJ software.

2.13 | Transendothelial electrical resistance (TEER) assay

TEER assay was conducted as previously reported,[25] with some modifications. The TEER values of the EC monolayer were measured using transwell chambers. MS1 cells were seeded into the upper compartment pre-coated with 1.5% gelatin (Corning, Life Sciences) to form an EC monolayer. *S. mutans* at an MOI of 1 was added to stimulate the MS1 cells and TEER values were measured using a Millicell®ERS-2 Electrical Resistance System (EMD Millipore Corporation, Billerica, MA, USA) at the indicated time points. The TEER values of the monolayer were calculated using the formula resistance (monolayer) = membrane area × [resistance (sample) − resistance (blank)].

2.14 | Transendothelial migration assay

Detailed descriptions of the methods are provided in Appendix S1.

2.15 | Mouse lung inflammation model

C57BL/6 mice (female, 6–7 weeks old, 17–20 g) were purchased from CLEA Japan (Tokyo, Japan). To create the mouse lung inflammation model, *S. mutans* (1×10^5 CFUs) was suspended in PBS and administered intravenously into the mouse tail vein every 2 days for a total of eight injections. PBS was injected as a control. Mice were sacrificed 15 days after the first administration and the lung tissues were excised for histological and genetic analyses. To examine the *S. mutans* infection to the lung ECs in vivo, mouse lung tissues were resected after 12 h and 24 h of a single dose of *S. mutans* (1×10^5 CFUs) injection. Then, the Gram stain and immunohistochemistry using an anti-CD31 antibody (Abcam, ab28364) were performed.

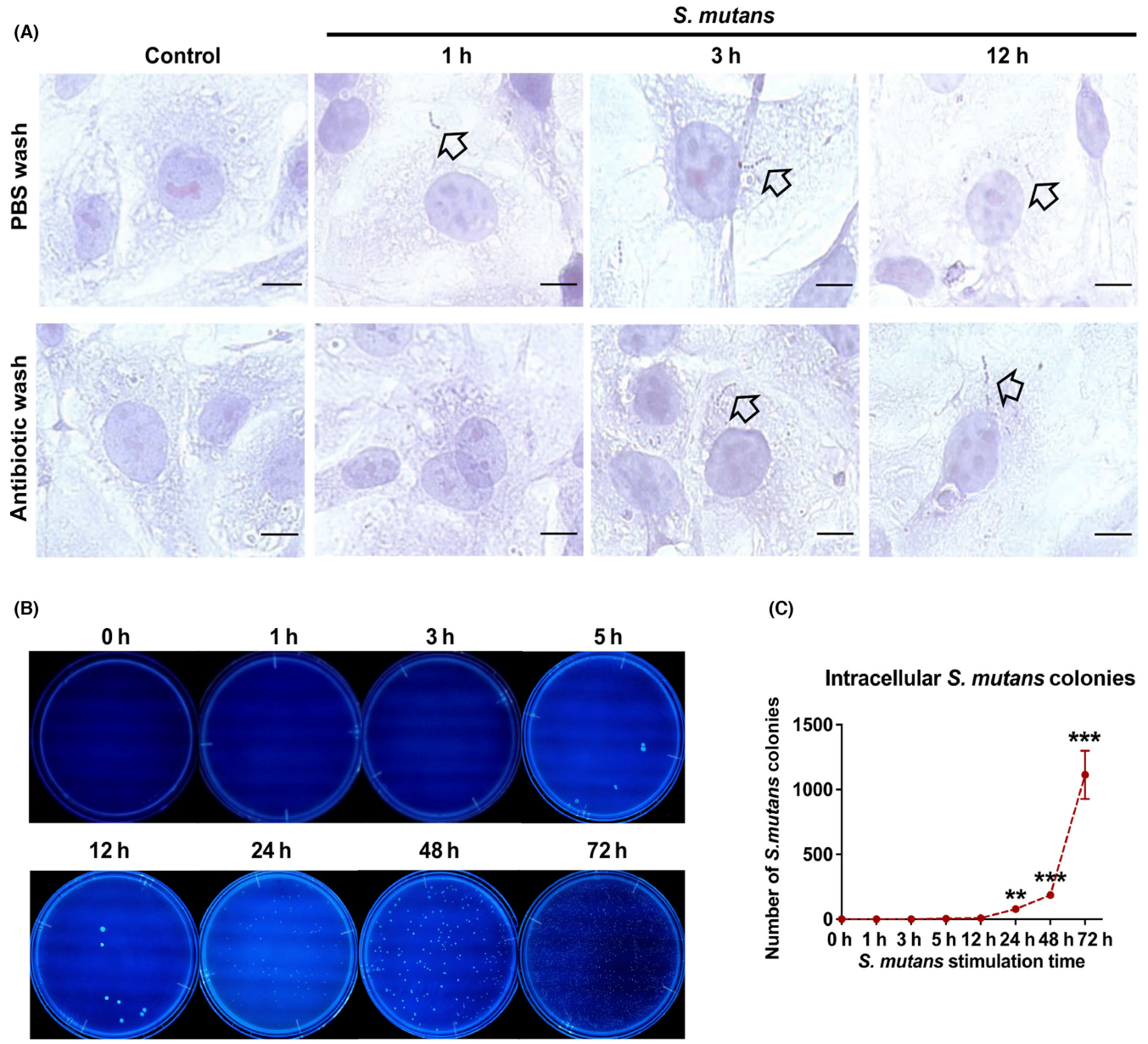

FIGURE 1 *S. mutans* invasion into ECs. (A) MS1 cells were stimulated by *S. mutans* for the indicated times and stained with Gram reagent. Representative images are shown: upper images of the PBS wash group and lower images of the antibiotic wash group after *S. mutans* stimulation; scale bars: 20 μm; arrowheads show *S. mutans*. (B, C) After *S. mutans* stimulation, MS1 was cultured in antibiotic-containing medium for 2 h; then, cells were lysed and cultured on brain–heart infusion (BHI) agar. (B) Representative images of *S. mutans* colonies on BHI agar. (C) The number of colonies was counted. Data represent the mean ± SD, $n = 3$; $^{**}p < 0.01$, $^{***}p < 0.001$; one-way ANOVA was used (C).

FIGURE 2 *S. mutans* induces inflammation in ECs and promotes tumor cell migration toward the ECs. (A) IL-6, IL-8, IL-1β, and TNF-α mRNA expression levels in MS1 were evaluated using real-time PCR after stimulation with *S. mutans* for 5 h. (B) Protein level of IL-6 in the cell culture supernatant was investigated using ELISA after stimulation with *S. mutans*. (C, D) The levels of phospho-NF-κB and NF-κB in MS1 were determined using western blot analysis after stimulation with *S. mutans* (C); the density was quantified using ImageJ software (D); β-actin was used as an internal control. (E) After treatment with the NF-κB inhibitor, MS1 cells were stimulated with *S. mutans* for 5 h, and IL-6, IL-8, IL-1β, and TNF-α mRNA expression levels were evaluated using real-time PCR. (F) Activated pathways upon *S. mutans* stimulation in MS1 cells were analyzed using RNA-seq. (G–I) Tumor cell migration toward ECs with or without *S. mutans* stimulation for 5 h was visualized using a migration assay. Schematic of migration assay (G); tdtomato-Luc2-expressing E0771 tumor cells migrating to the underside of the membrane were photographed; scale bars: 100 μm (H), and counted, $n = 5$ fields (I). Data represent the mean ± SD; $^{*}p < 0.05$, $^{**}p < 0.01$, $^{***}p < 0.001$; Student's *t*-test (A) and one-way ANOVA (B, D, E, I) were used.

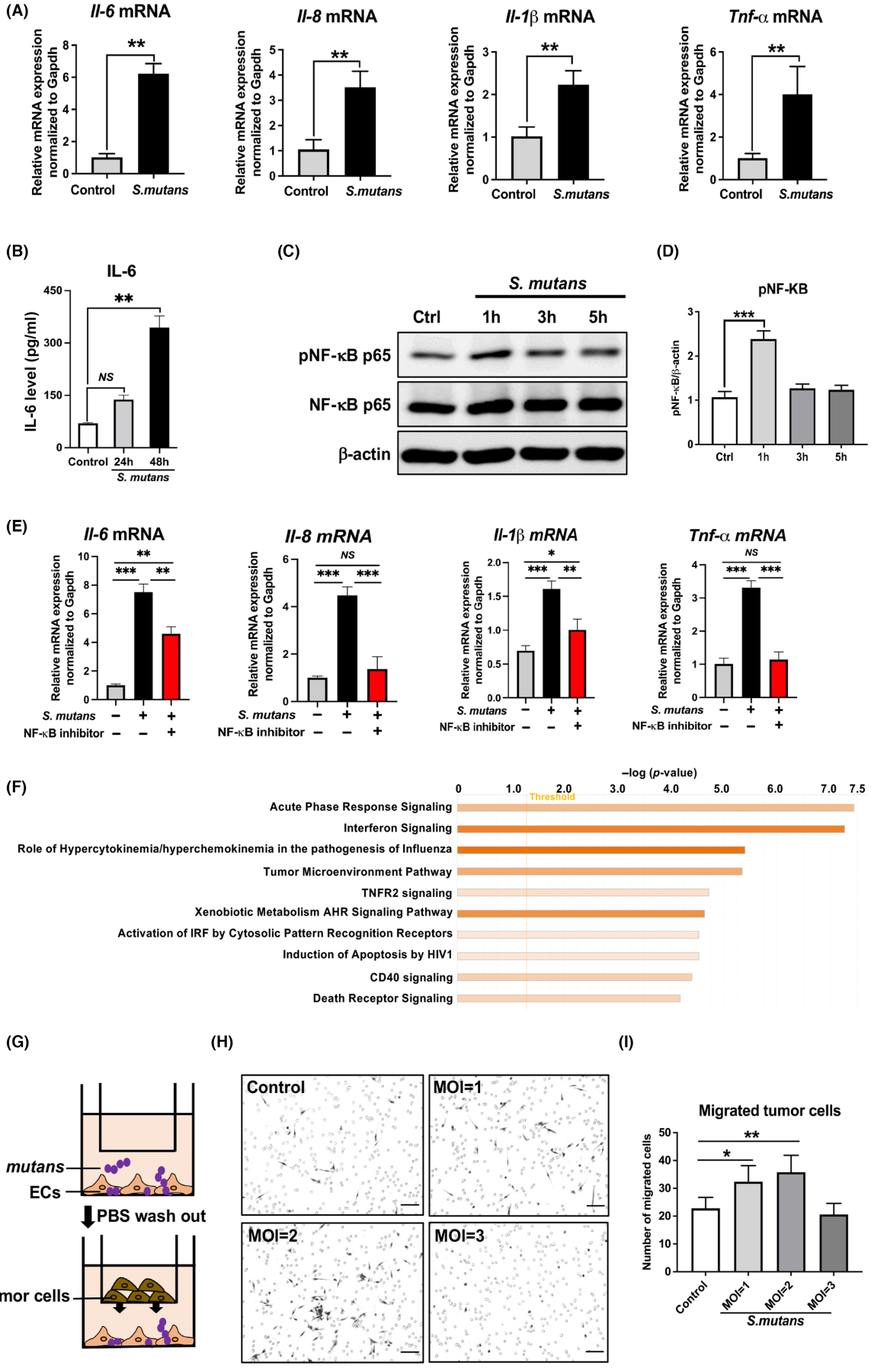

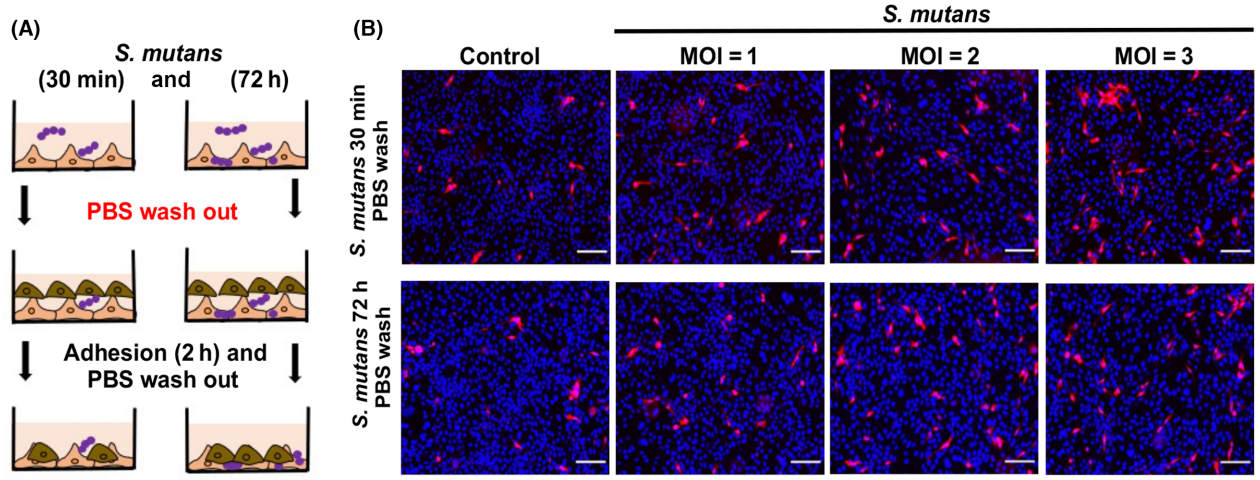

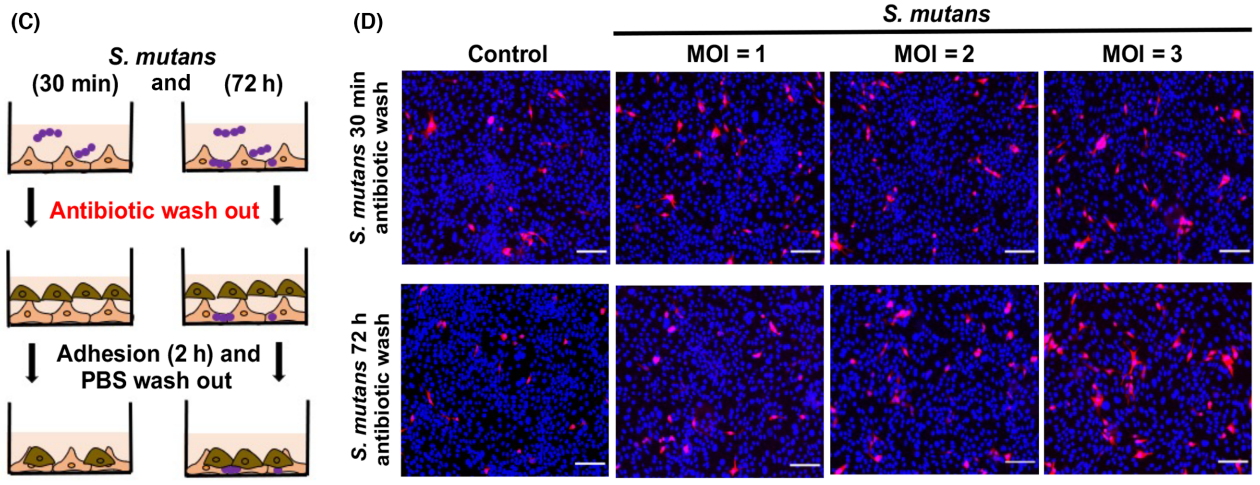

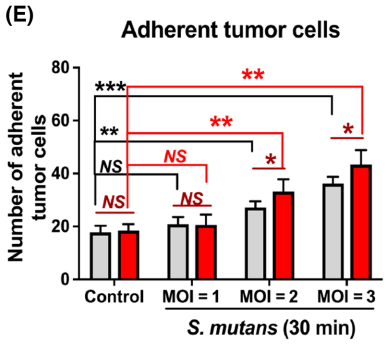

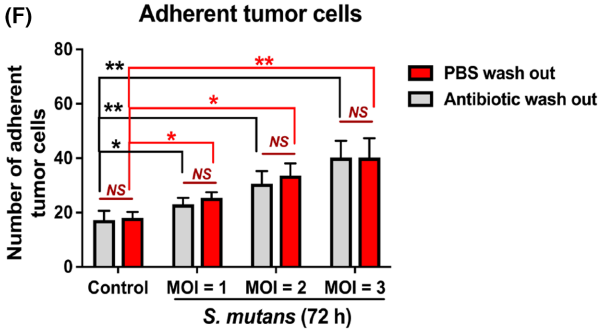

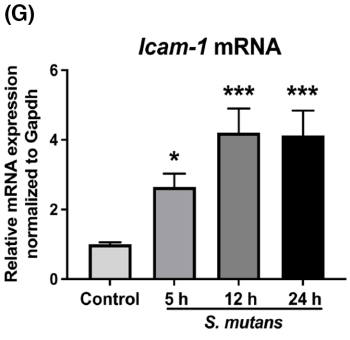

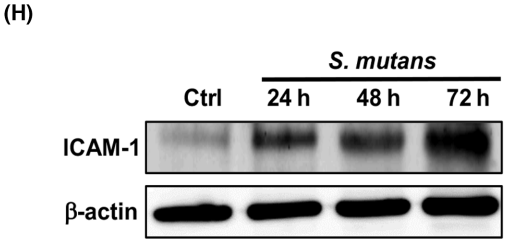

FIGURE 3 *S. mutans* promotes tumor cell–EC adhesion. (A–F) Tumor cell and EC adhesion with or without *S. mutans* stimulation for 30 min or 72 h were analyzed using an adhesion assay. Schematics of adhesion assay (A, C); adhered tdtomato-Luc2-expressing E0771 tumor cells (red) to *S. mutans*-stimulated ECs were photographed; scale bars: 100 μm; PBS wash group (B) and antibiotic wash group (D); adhered tumor cells to ECs after 30 min (E) or 72 h (F) of *S. mutans* stimulation were counted, $n = 5$ fields. (G) ICAM-1 mRNA expression in MS1 was evaluated using real-time PCR after stimulation with *S. mutans*, $n = 3$ real-time PCR runs. (H) The ICAM-1 protein level in MS1 was determined using western blot analysis after stimulation with *S. mutans*. Data represent the mean ± SD; NS, not significant, $^{*}p < 0.05$, $^{**}p < 0.01$, $^{***}p < 0.001$; two-way ANOVA (E, F) and one-way ANOVA (G) were used.

2.16 | In vivo vascular permeability model

Detailed descriptions of the methods are provided in Appendix S1.

2.17 | Mouse tumor metastasis model and treatment

C57BL/6 mice (female, 6–7 weeks old, 17–20 g) were exposed to *S. mutans* (PBS injection as control) as described for the previous inflammation model, followed by intravenous implantation of tdtomato-Luc2-expressing E0771 cells (2×10^5 cells), which were suspended in HBSS via the tail vein. At 1 week following tumor cell injection, mice were sacrificed via cervical dislocation after isoflurane anesthesia and the lungs were dissected. The bioluminescence IVIS imaging system (Caliper Life Science) was used to detect in vivo and ex vivo tumor metastasis in the lungs. The histological analysis of the lungs was performed using H&E staining.

The detailed descriptions of the anti-inflammatory drug treatment and NF-κB inhibition treatment methods are provided in Appendix S1.

2.18 | Histological analyses

Mouse lung tissues dissected from the inflammation and tumor metastasis models were processed by embedding in paraffin or optimal cutting temperature (OCT) compound. For the inflammation model, the paraffin-embedded lung tissues (4 μm) were stained with H&E, anti-mouse CD68 (Abcam, ab125212), and counterstained with hematoxylin. Frozen lung tissues were cut into 10-μm sections using a cryostat (Leica CM3050S, Leica Biosystems). Sections were fixed in 100% ice-cold acetone for 30 min and incubated with PBS containing 5% goat serum or 5% bovine serum albumin to avoid nonspecific binding. ICAM-1 and vascular endothelial (VE)-cadherin expression in the frozen sections was visualized using anti-mouse CD54 (BioLegend, 116101) and anti-mouse VE-cadherin (Abcam, ab33168), respectively, followed by counterstaining with hematoxylin. The images were scanned using a Virtual Slide Scanner NanoZoomer 2.0-HT (Tokyo, Japan). Frozen lung tissues were double-stained with allophycocyanin (APC) anti-mouse CD45 (BioLegend, 103112) and Alexa Fluor 448 anti-mouse CD31 (BioLegend, 102514) antibodies and counterstained with DAPI to determine the co-localization of CD31 and CD45-positive inflammatory cells. Images were acquired using a fluorescence microscope. Paraffin-embedded lung tissues in the tumor metastasis model were stained with H&E to detect metastasis. CD45-, CD68-, ICAM-1-, and VE-cadherin-positive staining was quantified using ImageJ software, the percentages of the positive areas were calculated to find the total area. Five fields per sample were quantified and values were averaged to obtain one value for each sample. Each group consisted of five mice.

2.19 | Statistical analyses

All data are presented as the means ± SD of three independent experiments. Student's *t*-test was used for comparison between two groups. One-way ANOVA or two-way ANOVA was performed for comparisons between multiple groups. Statistical analyses were performed using SPSS 19.0 software. A *p*-value < 0.05 was considered statistically significant.

3 | RESULTS

3.1 | *S. mutans* invasion into ECs

To evaluate the contribution of *S. mutans* to the development of vascular inflammation, we determined whether *S. mutans* invades ECs. After stimulation of ECs (MS1) with *S. mutans*, ECs were washed with PBS (PBS wash group) or antibiotic (antibiotic wash group) for 2 h to remove external *S. mutans*. Because *S. mutans* is a Gram-positive bacterium, we confirmed the existence of *S. mutans* using Gram staining.[26,27] *S. mutans* were detected in the PBS wash group after incubation with *S. mutans* for 1 h (Figure 1A, upper), whereas *S. mutans* in the antibiotic wash group were visualized after 3 h of *S. mutans* stimulation (Figure 1A, lower). The results indicated that the potential time required for *S. mutans* to adhere to the EC membrane surface was within 1 h. It required 3 h for *S. mutans* to invade the ECs. Furthermore, the intracellular *S. mutans* were quantified using a bacterial colony formation assay.[21] The intracellular-invading *S. mutans* were significantly increased with prolonged incubation time (Figure 1B,C), indicating that *S. mutans* can invade ECs.

3.2 | *S. mutans* induces inflammation in ECs and promotes tumor cells migration toward ECs

To determine whether *S. mutans* induces EC inflammation, we used real-time PCR to measure the expression of the inflammatory

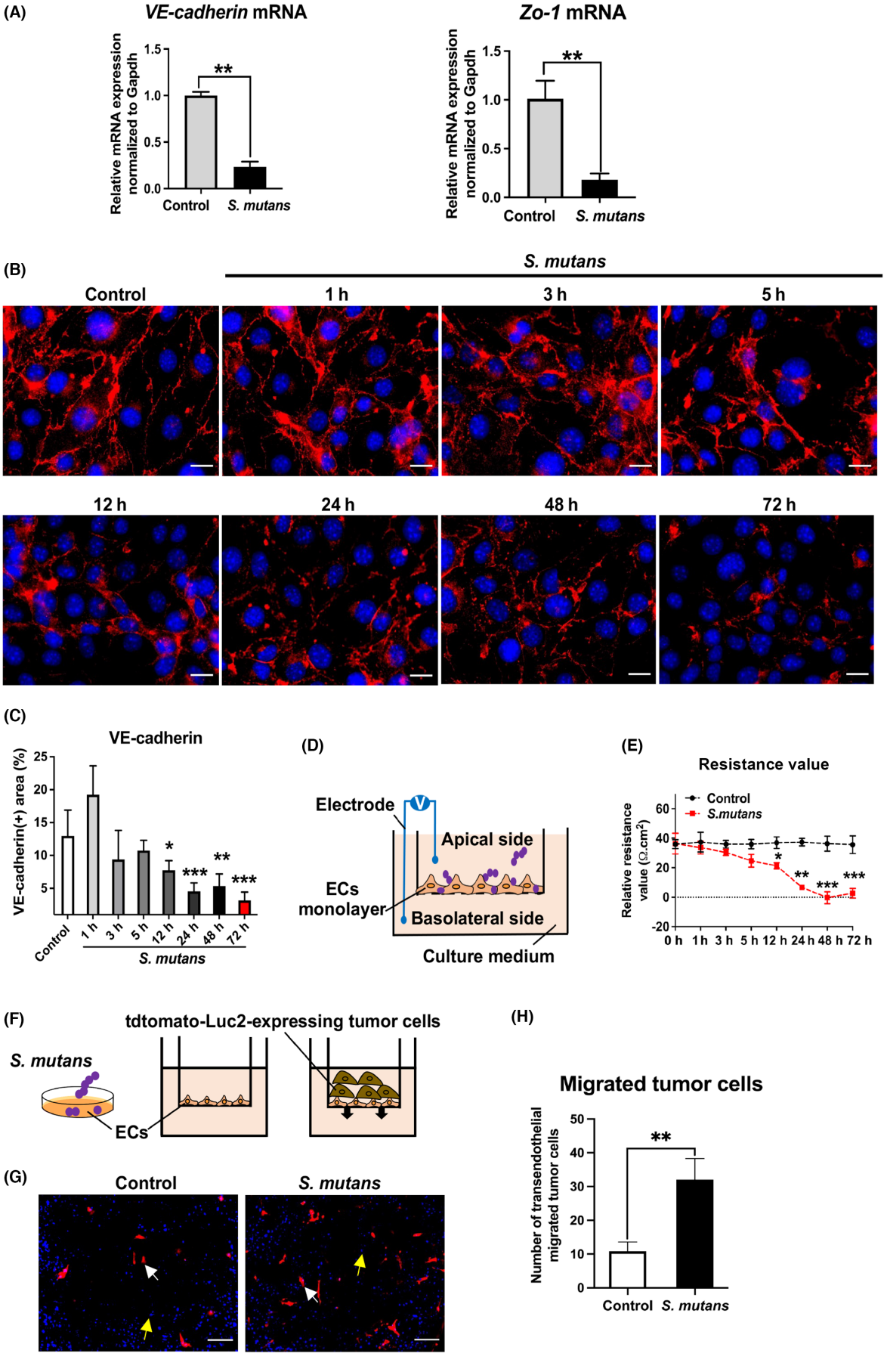

FIGURE 4 *S. mutans* disrupts vascular integrity. (A) VE-cadherin and ZO-1 mRNA expression in MS1 were evaluated using real-time PCR after stimulation with *S. mutans* for 5 h, $n = 3$ real-time PCR runs. (B, C) After stimulation with *S. mutans*, MS1 cells were stained with VE-cadherin (red) and counterstained with DAPI; representative images are shown; scale bars: 20 μm (B), and the VE-cadherin-positive areas were counted, $n = 5$ fields (C). (D, E) EC monolayer permeability was evaluated using the transepithelial electrical resistance (TEER) assay. Schematic of the TEER assay (D); MS1 cell monolayer was stimulated with *S. mutans*, and the TEER values of the monolayer were evaluated (E). (F–H) The migration of the tumor cells across the EC monolayer with or without *S. mutans* stimulation for 12 h was analyzed using a transendothelial migration assay. Schematic of the transendothelial migration assay (F); representative images of migrated tdtomato-Luc2-expressing E0771 tumor cells to the underside of the membrane were photographed, white arrowheads show migrated tumor cells, yellow arrowheads show migrated MS1 cells; scale bars: 100 μm (G), and counted, $n = 5$ fields (H). Data represent the mean ± SD; $^{*}p < 0.05$, $^{**}p < 0.01$, $^{***}p < 0.001$; Student's *t*-test (A, H), one-way ANOVA, compared with control group (C), and two-way ANOVA, compared with the control group at the same time point (E) were used.

cytokines, IL-6, IL-8, IL-1β, and TNF-α. These cytokines were significantly increased in ECs following stimulation with *S. mutans* (Figure 2A). Additionally, a high IL-6 level was detected in the culture supernatants after stimulation of ECs with *S. mutans* (Figure 2B). Moreover, an increase in IL-6 and IL-1β in ECs was identified by stimulation with *S. mutans* culture supernatant, but no upregulation in IL-8 and TNF-α (Figure S5A), indicating that *S. mutans* induces vascular inflammation mainly by directly invading ECs. As NF-κB is a transcriptional factor of proinflammatory genes, we determined whether NF-κB was activated by western blot analysis. *S. mutans*-stimulated ECs exhibited phosphorylated NF-κB (Figure 2C,D). NF-κB inhibition using NF-κB inhibitor, BAY11-7082, decreased the mRNA expression of these inflammatory cytokines (Figure 2E), suggesting that *S. mutans* induced inflammatory cytokines in ECs, which was regulated by NF-κB signaling. To identify enriched pathways in *S. mutans*-stimulated ECs, RNA-seq was performed in nonstimulated and *S. mutans*-stimulated ECs. Some pathways related to inflammation and cancer microenvironments were activated in *S. mutans*-stimulated ECs. The two most significantly enriched canonical pathways identified by IPA were interferon signaling ($p = 5.36 \times 10^{8}$) and acute phase response signaling ($p = 3.56 \times 10^{8}$) pathways (Figure 2F). These data suggest that *S. mutans* can be involved in inducing vascular inflammation and promoting tumor formation. Tumor cell migration toward *S. mutans*-stimulated ECs was evaluated using a cell migration assay (Figure 2G). Tumor cells migrated more efficiently toward *S. mutans*-stimulated ECs (Figure 2H,I). Additionally, we found that *S. mutans* mediates EMT gene expression (Figure S4A,B) and can promote tumor cell migration (Figure S4C,D). These results suggest that *S. mutans* is involved in tumor cell migration toward ECs and promotes extravasation.

3.3 | *S. mutans* promotes tumor cell–EC adhesion

In the process of tumor cell extravasation, tumor cells make contact with ECs. The association of *S. mutans* with tumor cell–EC adhesion was determined using an adhesion assay (Figure 3A–F). After the indicated times of *S. mutans* stimulation of the ECs, one group was washed with PBS to remove the *S. mutans* from the culture medium (Figure 3A,B) and the other group was washed with antibiotics to remove both the cell surface adherent S. *mutans* and the *S. mutans* in the culture medium (Figure 3C,D). The number of adherent tumor cells to the ECs was significantly increased by the *S. mutans* number and in a stimulation time-dependent manner (Figure 3E,F). After exposure to *S. mutans* for 30 min, the number of EC-adherent tumor cells was significantly higher in the PBS wash group than in the antibiotics wash group (Figure 3B upper, D upper, E). In contrast, no difference was observed between the PBS wash group and the antibiotic wash group at 72 h after *S. mutans* stimulation (Figure 3B lower, D lower, F). Combined with the Gram staining results that showed that *S. mutans* merely adhered to the EC membrane within 1 h of *S. mutans* stimulation, followed by entering the ECs after 3 h of stimulation (Figure 1A), these results indicated that both cell surface and invading *S. mutans* are involved in promoting tumor cell adhesion to ECs. The intercellular adhesion molecule ICAM-1 is involved in tumor cell adhesion to blood vessels.[28] We observed markedly enhanced expression of ICAM-1 at the mRNA level and protein level in *S. mutans*-stimulated ECs (Figure 3G,H). Moreover, elevated ICAM-1 mRNA levels were observed in ECs after being stimulated with *S. mutans* culture supernatant (Figure S5B), reinforcing the idea that invasion and adhesion of *S. mutans* to ECs may upregulate ICAM-1 expression in ECs to contribute to promoting tumor cell–EC adhesion. These data suggest that *S. mutans* regulates tumor cell adhesion to the endothelium by activating ICAM-1 in the ECs.

3.4 | *S. mutans* disrupts vascular integrity

Vascular leakage is responsible for tumor cell extravasation across the endothelium for metastasis to secondary organs.[29] Therefore, we compared the expression of the endothelial adhesion molecules, VE-cadherin and ZO-1, in *S. mutans*-stimulated ECs and nonstimulated ECs. Both VE-cadherin and ZO-1 mRNA expression was significantly decreased in ECs following *S. mutans* stimulation (Figure 4A). Conversely, no reduction in VE-cadherin and ZO-1 levels was observed in ECs stimulated with *S. mutans* secretions (Figure S5C), suggesting that the direct contact of ECs and *S. mutans* is important for changes in gene expression. Immunofluorescence staining data indicated that VE-cadherin expression in ECs was significantly reduced with increased *S. mutans* stimulation time (Figure 4B,C). The TEER assay revealed a reduction in the TEER values in the *S. mutans*-stimulated EC monolayer (Figure 4D,E). Most importantly, transendothelial migration of tumor

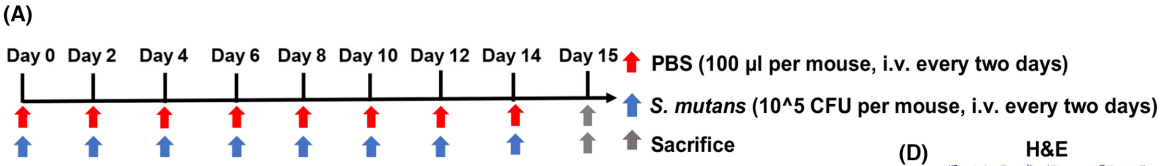

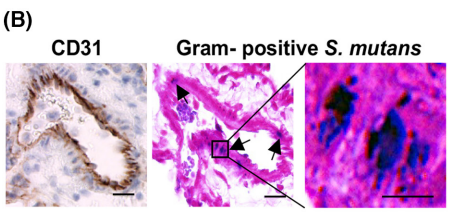

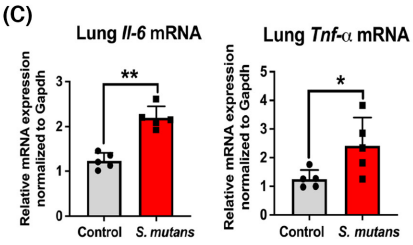

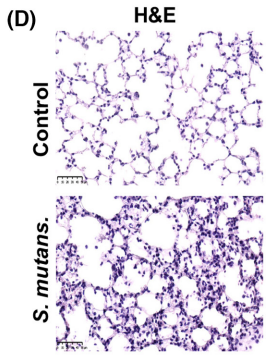

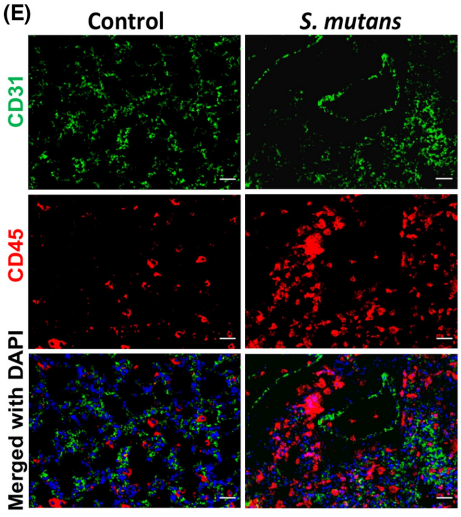

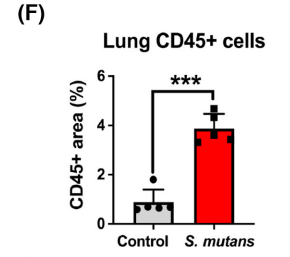

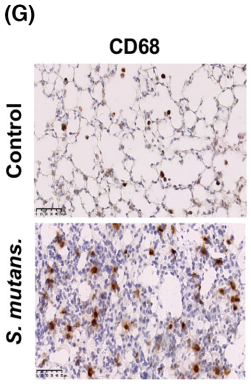

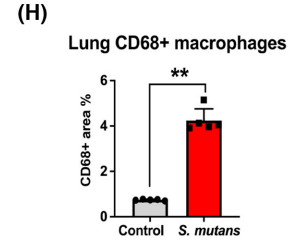

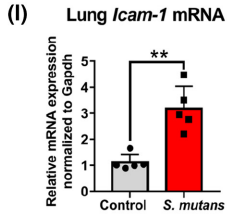

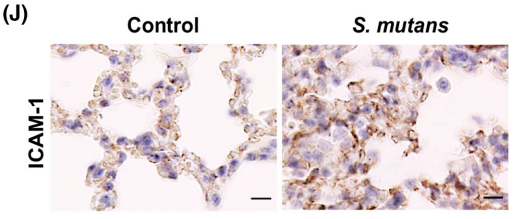

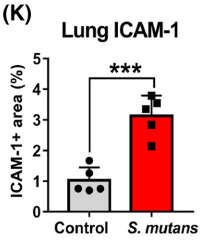

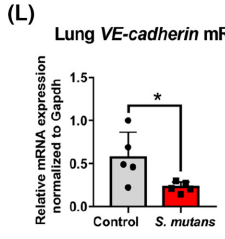

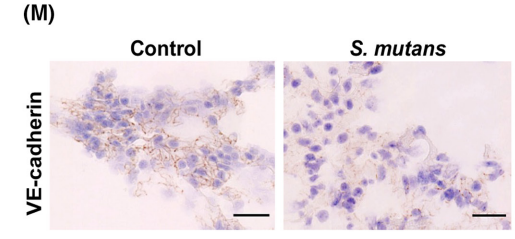

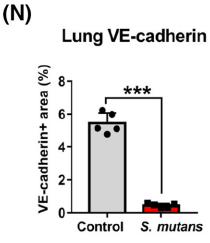

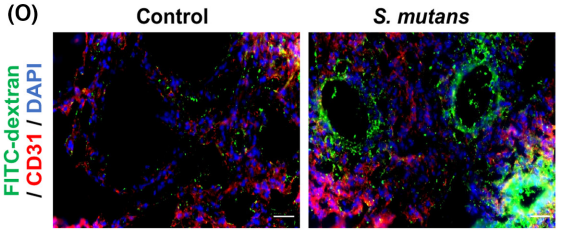

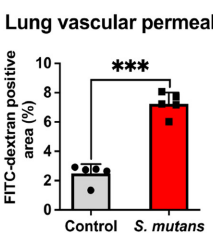

FIGURE 5 *S. mutans* induce inflammation in the lungs. (A) Experimental design of *S. mutans* inducing lung inflammation in vivo. (B) Representative images of *S. mutans* infection in lung ECs using Gram staining and CD31 immunohistochemistry after 12 h of *S. mutans* intravenous injection, black arrowheads show Gram-positive *S. mutans*; scale bars for low magnification, 50 μm: for high magnification, 20 μm. (C) IL-6 and TNF-α mRNA expression in the lung tissues was evaluated by real-time PCR; $n = 3$ real-time PCR replicates per mouse. (D) Representative images of lung tissues stained with H&E; scale bars: 50 μm. (E, F) The lung tissues were double-stained with CD31 (green)/CD45 (red); representative images were photographed; scale bars: 50 μm (E), and the CD45-positive areas were counted, $n = 5$ fields (F). (G, H) Macrophages in the lung tissues were stained with CD68; representative images were photographed; scale bars: 50 μm (G), and the CD68-positive areas were quantified, $n = 5$ fields (H). (I) ICAM-1 mRNA expression in lung tissues by real-time PCR, $n = 3$ real-time PCR replicates per mouse. (J, K) The lung tissues were stained with ICAM-1; representative images were photographed; scale bars: 50 μm (J), and the ICAM-1-positive areas were counted, $n = 5$ fields (K). (L) VE-cadherin mRNA expression in lung tissues by real-time PCR, $n = 3$ real-time PCR replicates per mouse. (M, N) The lung tissues were stained with VE-cadherin; representative images were photographed; scale bars: 20 μm (M), and the VE-cadherin-positive areas were counted, $n = 5$ fields (N). (O, P) Mice were intravenously injected with 40-kDa FITC-dextran, which were left to circulate. Lung tissues were collected and stained with CD31 (red) and DAPI (blue) to visualize blood vessels and nuclei, scale bars: 50 μm (O); the FITC-dextran fluorescence intensity was quantified, $n = 5$ fields (P). Data represent the mean ± SD; $^{*}p < 0.05$, $^{**}p < 0.01$, $^{***}p < 0.001$; Student's *t*-test (C, F, H, I, K, L, N, P) was used, five mice per group.

cells across the EC monolayer was significantly increased by *S. mutans* stimulation in ECs (Figure 4F,G), indicating the enhanced vascular leakage by *S. mutans*. Taken together, these data suggest that *S. mutans* disrupts vascular integrity by downregulation of adhesion molecules in the ECs, supporting tumor cell transendothelial migration.

3.5 | *S. mutans* induces inflammation in the lungs

To determine whether *S. mutans* induces vascular inflammation in vivo, *S. mutans* was administered intravenously to C57BL/6 female mice, whereas PBS was injected as a control (Figure 5A). Vascular inflammation was assessed in the lung tissues. The infection of *S. mutans* to the lung ECs was confirmed after 12 h of *S. mutans* injection (Figure 5B). The expression of the inflammatory cytokines, IL-6 and TNF-α, was upregulated in the *S. mutans* group compared with the control group, suggesting that *S. mutans* causes lung inflammation in vivo (Figure 5C). In addition, lung tissues were infiltrated with inflammatory cells and an abnormal structure of the lung alveoli was evident, with thickening alveolar walls in the *S. mutans* group (Figure 5D). CD45 is a good marker of the inflammatory response and is highly expressed in immune cells.[30,31] Double immunofluorescent staining of CD31 and CD45 revealed a significant increase in CD45-positive inflammatory cells in the lungs of the *S. mutans* group accompanied by the accumulation of CD45-positive inflammatory cells around the CD31-positive area (Figure 5E,F). Furthermore, we quantitatively analyzed macrophages, which are prominent during chronic inflammation. The number of CD68-positive macrophages was significantly increased in the lungs of the *S. mutans* group (Figure 5G,H), suggesting that *S. mutans* elicits chronic lung inflammation in vivo. The expression of ICAM-1 mRNA and protein in the lungs was analyzed by real-time PCR and immunohistochemistry, respectively (Figure 5I–K). Both ICAM-1 mRNA level (Figure 5I) and ICAM-1-positive staining (Figure 5J,K) were increased in the *S. mutans* group. Furthermore, the expression of VE-cadherin was significantly reduced in the *S. mutans* group (Figure 5L–N). To address whether the reduction of VE-cadherin causes vascular hyperpermeability, lung vascular permeability was studied through intravenous injection of 40-kDa FITC-dextran to the mice. Fluorescence imaging showed higher diffusion of the FITC-dextran in the *S. mutans* group than in the control group (Figure 5O,P). Together, these data indicated that *S. mutans* induces chronic lung inflammation accompanied by enhanced intercellular adhesions and reduced endothelial adherens junctions, as well as vascular hyperpermeability.

3.6 | *S. mutans* promotes tumor metastasis to the lungs

In vitro data showed that *S. mutans* promotes the migration and adhesion of tumor cells to ECs. Therefore, we determined whether *S. mutans*-induced vascular inflammation affects tumor metastasis in vivo. We injected *S. mutans* intravenously, as in the previous in vivo experiments, followed by implantation of murine breast carcinoma tdtomato-Luc2-expressing E0771 cells via the tail vein (Figure 6A). The *S. mutans* group exhibited significantly increased lung metastatic tumors as determined by in vivo and ex vivo imaging 1 week following tumor cell injection (Figure 6B–D). Metastatic tumor cells in the lungs were confirmed histologically by H&E staining (Figure 6E). To find in vivo evidence that *S. mutans* promotes tumor metastasis by inducing inflammation through NF-κB signaling, anti-inflammatory drug, aspirin, or NF-κB inhibitor was treated in the proinflammatory stage, respectively. Consistent with the in vitro data, significant regression of lung metastasis was observed in the mice along with aspirin (Figure 6F–I) or NF-κB inhibitor (Figure 6J–M). These results suggest that *S. mutans* promotes tumor metastasis to the lungs through the induction of vascular inflammation (Figure 7).

4 | DISCUSSION

In this study, we demonstrated that *S. mutans*, a major oral bacterium responsible for dental caries, promotes tumor metastasis by invading the blood circulation (Figure 7). To our knowledge, this is the first report demonstrating that oral bacteria can promote tumor metastasis by inducing vascular inflammation at distant organs. This suggests that oral bacteria may represent a risk factor for tumor metastasis.

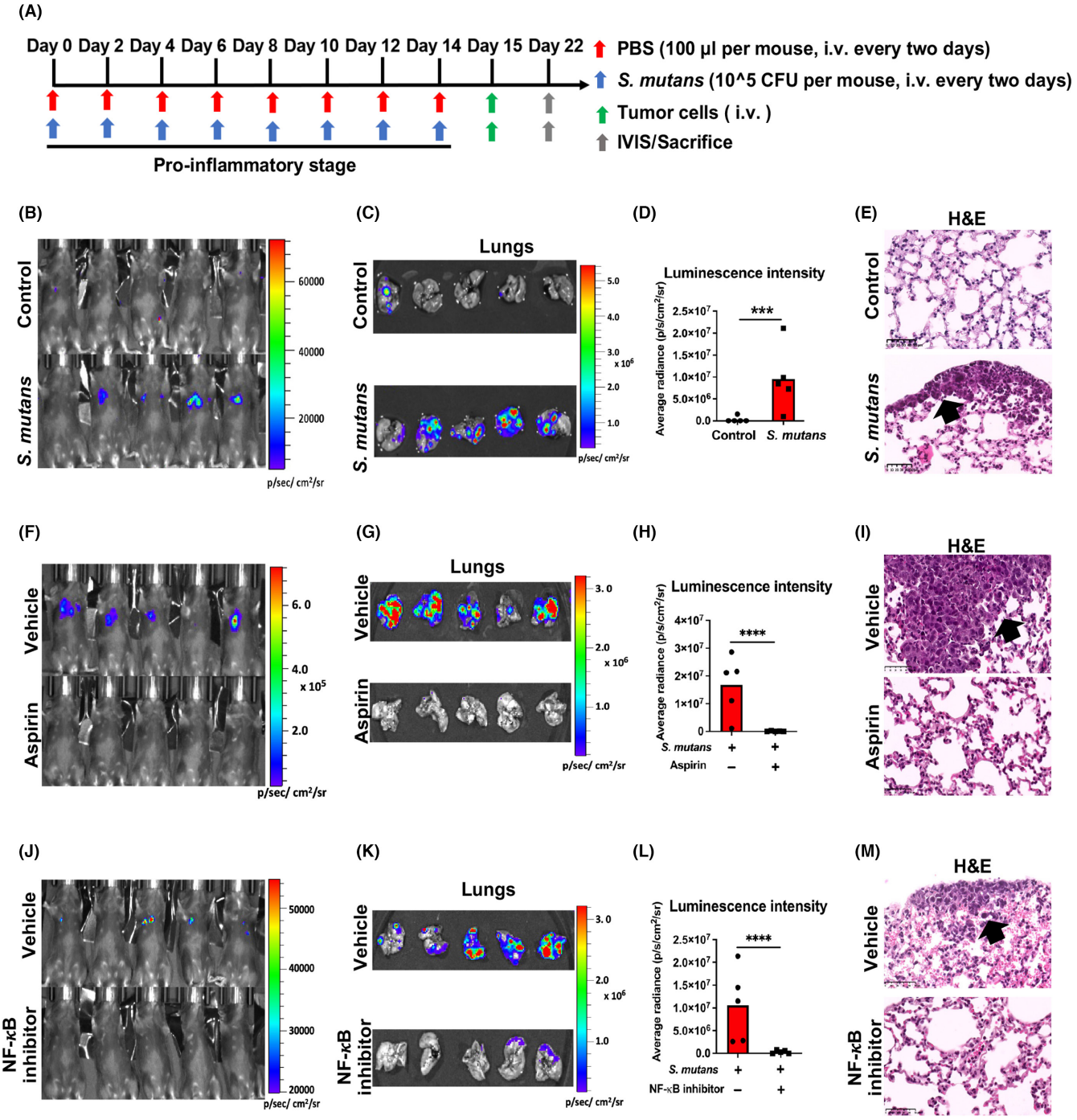

FIGURE 6 *S. mutans* promotes tumor metastasis to the lungs. (A) The experimental design of *S. mutans*-promoting tumor metastasis. (B–D) Lung metastatic tumor cell luminescence intensity was detected using an IVIS Spectrum instrument; the images of in vivo metastatic lung tumors (B), ex vivo metastatic lung tumors (C), and quantification of ex vivo luminescence intensity (D). (E) Representative images of lung metastatic tumors stained with H&E; arrowheads show metastatic tumor cells; scale bars: 50 µm. (F–I) Anti-inflammatory drug, aspirin, treatment hampers tumor metastasis of the lungs in the *S. mutans*-promoting tumor metastasis model. Mice were treated with vehicle as a control or 100 mg/kg aspirin orally during the proinflammatory stage, followed by administration of tdtomato-Luc2-expressing E0771 tumor cells intravenously; representative images of in vivo metastatic lung tumors (F), ex vivo metastatic lung tumors (G), and quantification of ex vivo luminescence intensity (H). (I) Representative images of metastatic lung tumors stained with H&E; arrowheads show metastatic tumor cells; scale bars: 50 µm. (J–M) NF-κB inhibitor treatment hampers tumor metastasis in the lungs in the *S. mutans*-promoting tumor metastasis model. Mice were treated with vehicle as the control or 10 mg/kg NF-κB inhibitor BAY-117082 intraperitoneally during the proinflammatory stage, followed by administration of tdtomato-Luc2-expressing E0771 tumor cells intravenously; representative images of in vivo metastatic lung tumors (J), ex vivo metastatic lung tumors (K), and quantification of ex vivo luminescence intensity (L). (M) Representative images of metastatic lung tumors stained with H&E; arrowheads show metastatic tumor cells; scale bars: 50 µm. Data represent the mean; ***$p < 0.001$; ****$p < 0.0001$; Student's *t*-test was used, five mice per group (D, H, L).

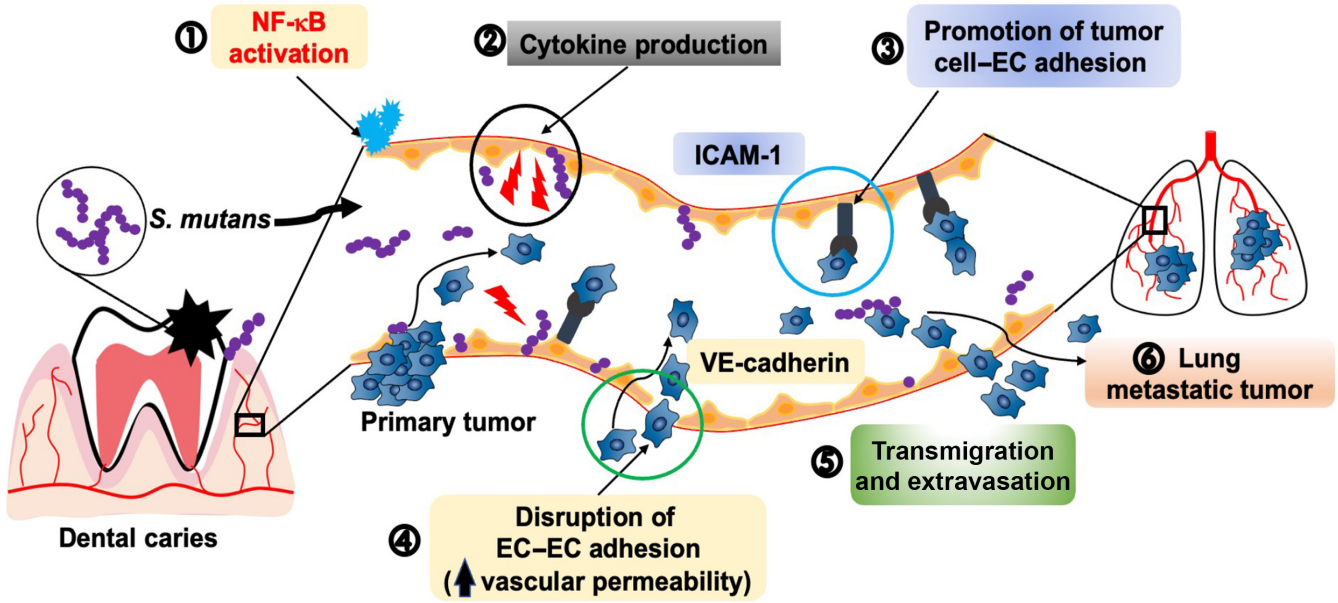

FIGURE 7 Schematic illustrating the mechanism of *S. mutans*-promoting tumor metastasis to the lungs. *S. mutans* invasion into the blood vessels induces vascular inflammation through NF-κB signaling, promotes the tumor cell–EC adhesion, disrupts the vascular integrity, and further promotes tumor metastasis to the lungs.

An important issue in the field of tumor metastasis is whether and how oral bacteria are potentially involved in tumor metastasis. *S. mutans* is a representative oral bacterium that is highly relevant to cardiovascular inflammation as it may enter the bloodstream through inflamed gums or periodontal pockets.[32,33] Therefore, we used *S. mutans* to study oral bacteria-associated vascular inflammation and its association with tumor metastasis. Previous studies used high concentrations of *S. mutans*[12,21]; however, we determined the effects of *S. mutans* on ECs at low MOIs to mimic the physiological process of *S. mutans* invading the circulation, because too many oral bacteria entering the bloodstream at once is uncommon during ordinary dental treatment or daily oral hygiene practices.[34] Consistent with a previous report,[35] our study indicated that *S. mutans* induces vascular inflammation, even at low MOIs.

During the process of hematogenous metastasis, circulating tumor cells adhere to the endothelium and prepare for extravasation.[20] *S. mutans*-induced IL-8 upregulation may serve as a chemoattractant for tumor cell migration toward the endothelium. Because it has been reported that high levels of the chemokine showed antitumor activity,[36,37] and high MOIs of oral bacteria inhibit the epithelial cell migration,[38,39] this may explain why stimulation with *S. mutans* at an MOI of 3 produced no significant difference in promoting tumor cell migration (Figure 2H,I). Intercellular adhesion molecules regulate tumor cell–EC adhesion and support the transendothelial extravasation process. Particularly, ICAM-1 is a molecule that is highly expressed during the inflammatory response.[40,41] In addition, the abnormal expression of intercellular adhesion molecules is a hallmark of tumor metastasis.[42] In our study, the significant increase of ICAM-1 observed in *S. mutans*-stimulated ECs may explain the fact that more tumor cells adhere to *S. mutans*-stimulated ECs. This suggests that *S. mutans*-induced vascular inflammation modulates tumor cell extravasation by enhancing ICAM-1 signaling.

The endothelium regulates tumor cell extravasation through its selective semipermeable barrier. The essential molecule that governs the opening and closing of the endothelial barrier is VE-cadherin. EC-mediated vascular permeability is enhanced dramatically in response to inflammation.[43] In addition, extracellular stimuli, such as bacterial invasion, results in impaired vascular permeability.[44,45] In this study, we proposed that *S. mutans*-stimulated ECs cause VE-cadherin cleavage in response to oral bacteria-associated vascular inflammation. Moreover, VE-cadherin attenuation results in disrupted vascular integrity. Our results show that the endothelial barrier is dysregulated by *S. mutans* invading ECs, leading to the hyperpermeability of the blood vessels, therefore elevating transendothelial migration of tumor cells. Based on this finding, we hypothesize that *S. mutans* promotes hematogenous metastasis by enhancing vascular permeability.

Inflammation in the tumor environment, especially chronic inflammation, responds to inflammation-initiating stimuli to promote tumor growth.[46–49] Previous reports have highlighted the role of chronic inflammation in primary tumors[50,51]; however, our study was focused on the role of oral bacteria-induced vascular inflammation in tumor metastasis to distant organs. We detected vascular and chronic inflammation in the lungs by intravenously administering *S. mutans* to the mice. Gut microbiota-induced inflammation directs gastrointestinal cancer development.[52,53] Intestinal bacterial dissemination induced by gut vascular leakage promotes colorectal cancer metastasis.[54] These reports suggest that bacteria-associated inflammation and vascular disruption support metastasis. Furthermore, one study found large numbers of bacteria in human breast carcinoma tissues.[55] Therefore, in this study, we examined the contribution of *S. mutans* in promoting breast cancer

metastasis to the lungs. We discovered that *S. mutans*, oral bacteria, actively mediate hematogenous metastasis by initiating an inflammatory response in distant organs through NF-κB signaling.

In this study, we primarily focused on oral bacteria-associated inflammation in distant organs. It remains unclear whether *S. mutans* facilitated the process of tumor cells detaching from primary tumors or assisted in tumor cell intravasation. In addition, oral bacteria are in the dynamic balance. Whether the periodontitis pathogen *Porphyromonas gingivalis* or other subsets of oral bacteria share the same mechanism in promoting tumor metastasis remains to be determined. Moreover, *S. mutans* injection induces hepatitis in the mice (data not shown) and it remains unclear whether *S. mutans* also promotes tumor metastasis to the liver.

Postoperative pneumonia frequently occurs in hospitalized patients and is intimately associated with postoperative mortality.[56] Oral bacteria increase the risk of postoperative pneumonia and professional oral hygiene practices serve to minimize the risk of postoperative pneumonia in lung and esophageal cancer.[57,58] Our findings reveal a novel role of oral bacteria in promoting tumor metastasis. They reinforce the need for professional oral hygiene management in patients with cancer in terms of avoiding not only postoperative pneumonia but also tumor metastasis.

ACKNOWLEDGMENTS

We would like to thank Dr. Y. Umeyama, Dr. MA. Towfik, Ms. M. Sasaki, and Ms. Y. Suzuki for their technical assistance with the experiments.

FUNDING INFORMATION

This research was supported by JSPS Grants-in-Aid for Scientific Research to NM (JP18K09715), YH (JP18H02891) and KH (JP18H02996), Grants from the Japan Agency for Medical Research and Development (AMED) to NM (JP18ck0106198h0003) and KH (JP19ck0106406h0002), JST SPRING (JPMJSP2119).

CONFLICT OF INTEREST

The authors declare no conflicts of interest. KH is a current Editorial Board member of *Cancer Science*.

ETHICS STATEMENT

Approval of the research protocol by an Institutional Reviewer Board: N/A.

Informed Consent: N/A.

Registry and the Registration No. of the study/trial: N/A.

Animal Studies: All animal experiments were approved by the animal research authorities of Hokkaido University. The authors followed the Animal Research: Reporting of In Vivo Experiments (ARRIVE) guidelines for animal studies.

ORCID

Li Yu https://orcid.org/0000-0002-5874-055X
Yasuhiro Hida https://orcid.org/0000-0003-1759-4215
Kyoko Hida https://orcid.org/0000-0002-7968-6062

REFERENCES

1. Ferlay J, Colombet M, Soerjomataram I, et al. Estimating the global cancer incidence and mortality in 2018: GLOBOCAN sources and methods. *Int J Cancer*. 2019;144:1941-1953.
2. Balkwill F, Mantovani A. Inflammation and cancer: back to Virchow? *Lancet*. 2001;357:539-545.
3. Coussens LM, Werb Z. Inflammation and cancer. *Nature*. 2002;420:860-867.
4. DiGiacomo JW, Gilkes DM. Tumor hypoxia as an enhancer of inflammation-mediated metastasis: emerging therapeutic strategies. *Target Oncol*. 2018;13:157-173.
5. Neufert C, Heichler C, Brabletz T, et al. Inducible mouse models of colon cancer for the analysis of sporadic and inflammation-driven tumor progression and lymph node metastasis. *Nat Protoc*. 2021;16:61-85.
6. Zeeshan R, Mutahir Z. Cancer metastasis - tricks of the trade. *Bosn J Basic Med Sci*. 2017;17:172-182.
7. Tang Q, Su Z, Gu W, Rustgi AK. Mutant p53 on the path to metastasis. *Trends Cancer*. 2020;6:62-73.
8. Lemos JA, Palmer SR, Zeng L, et al. The biology of *Streptococcus mutans*. *Microbiol Spectr*. 2019;7(1):1-7.
9. Hong SW, Baik JE, Kang SS, Yun CH, Seo DG, Han SH. Lipoteichoic acid of *Streptococcus mutans* interacts with toll-like receptor 2 through the lipid moiety for induction of inflammatory mediators in murine macrophages. *Mol Immunol*. 2014;57:284-291.
10. Kim JS, Kim KD, Na HS, et al. Tumor necrosis factor-α and interleukin-1β expression pathway induced by *Streptococcus mutans* in macrophage cell line RAW 264.7. *Mol Oral Microbiol*. 2012;27:149-159.
11. Chamat-Hedemand S, Dahl A, Østergaard L, et al. Prevalence of infective endocarditis in streptococcal bloodstream infections is dependent on streptococcal species. *Circulation*. 2020;142:720-730.
12. Nomura R, Otsugu M, Hamada M, et al. Potential involvement of *Streptococcus mutans* possessing collagen binding protein Cnm in infective endocarditis. *Sci Rep*. 2020;10:19118.
13. Maishi N, Hida K. Tumor endothelial cells accelerate tumor metastasis. *Cancer Sci*. 2017;108:1921-1926.
14. Torii C, Maishi N, Kawamoto T, et al. miRNA-1246 in extracellular vesicles secreted from metastatic tumor induces drug resistance in tumor endothelial cells. *Sci Rep*. 2021;11:13502.
15. Cong L, Maishi N, Annan DA, et al. Inhibition of stromal biglycan promotes normalization of the tumor microenvironment and enhances chemotherapeutic efficacy. *Breast Cancer Res*. 2021;23:51.
16. Annan DA, Kikuchi H, Maishi N, Hida Y, Hida K. Tumor endothelial cell-a biological tool for translational cancer research. *Int J Mol Sci*. 2020;21:3238.
17. Maishi N, Sakurai Y, Hatakeyama H, et al. Novel antiangiogenic therapy targeting biglycan using tumor endothelial cell-specific liposomal siRNA delivery system. *Cancer Sci*. 2022;113:1855-1867.
18. Nagata E, Oho T. Invasive *Streptococcus mutans* induces inflammatory cytokine production in human aortic endothelial cells via regulation of intracellular toll-like receptor 2 and nucleotide-binding oligomerization domain 2. *Mol Oral Microbiol*. 2017;32:131-141.
19. Quail DF, Joyce JA. Microenvironmental regulation of tumor progression and metastasis. *Nat Med*. 2013;19:1423-1437.
20. Maishi N, Ohba Y, Akiyama K, et al. Tumour endothelial cells in high metastatic tumours promote metastasis via epigenetic dysregulation of biglycan. *Sci Rep*. 2016;6:28039.
21. Alves LA, Ganguly T, Harth-Chú ÉN, et al. PepO is a target of the two-component systems VicRK and CovR required for systemic virulence of *Streptococcus mutans*. *Virulence*. 2020;11:521-536.
22. Ohga N, Hida K, Hida Y, et al. Inhibitory effects of epigallocatechin-3 gallate, a polyphenol in green tea, on tumor-associated endothelial cells and endothelial progenitor cells. *Cancer Sci*. 2009;100:1963-1970.

23. Tsumita T, Maishi N, Annan DA, et al. The oxidized-LDL/LOX-1 axis in tumor endothelial cells enhances metastasis by recruiting neutrophils and cancer cells. *Int J Cancer*. 2022;151:944-956.
24. Kurosu T, Ohga N, Hida Y, et al. HuR keeps an angiogenic switch on by stabilising mRNA of VEGF and COX-2 in tumour endothelium. *Br J Cancer*. 2011;104:819-829.
25. van der Helm MW, Odijk M, Frimat JP, et al. Direct quantification of transendothelial electrical resistance in organs-on-chips. *Biosens Bioelectron*. 2016;85:924-929.
26. Boerner DF, Zwadyk P. The value of the sputum gram's stain in community-acquired pneumonia. *Jama*. 1982;247:642-645.
27. Collins JP, Westblade LF, Anderson EJ. Gram-positive diplococci in a cerebrospinal fluid gram stain. *Open Forum Infect Dis*. 2016;3:ofw206.
28. Yang L, Froio RM, Sciuto TE, Dvorak AM, Alon R, Luscinskas FW. ICAM-1 regulates neutrophil adhesion and transcellular migration of TNF-alpha-activated vascular endothelium under flow. *Blood*. 2005;106:584-592.
29. Azzi S, Hebda JK, Gavard J. Vascular permeability and drug delivery in cancers. *Front Oncol*. 2013;3:211.
30. Russo AJ, Vasudevan SO, Méndez-Huergo SP, et al. Intracellular immune sensing promotes inflammation via gasdermin D-driven release of a lectin alarmin. *Nat Immunol*. 2021;22:154-165.
31. Irie-Sasaki J, Sasaki T, Matsumoto W, et al. CD45 is a JAK phosphatase and negatively regulates cytokine receptor signalling. *Nature*. 2001;409:349-354.
32. Kesavalu L, Lucas AR, Verma RK, et al. Increased atherogenesis during *Streptococcus mutans* infection in ApoE-null mice. *J Dent Res*. 2012;91:255-260.
33. Otsugu M, Nomura R, Matayoshi S, Teramoto N, Nakano K. Contribution of *Streptococcus mutans* strains with collagen-binding proteins in the presence of serum to the pathogenesis of infective endocarditis. *Infect Immun*. 2017;85:e00401-17.
34. Sconyers JR, Crawford JJ, Moriarty JD. Relationship of bacteremia to toothbrushing in patients with periodontitis. *J Am Dent Assoc*. 1973;87:616-622.
35. Nagata E, de Toledo A, Oho T. Invasion of human aortic endothelial cells by oral viridans group streptococci and induction of inflammatory cytokine production. *Mol Oral Microbiol*. 2011;26:78-88.
36. Hu Z, Chen J, Zhou S, et al. Mouse IP-10 gene delivered by folate-modified chitosan nanoparticles and dendritic/tumor cells fusion vaccine effectively inhibit the growth of hepatocellular carcinoma in mice. *Theranostics*. 2017;7:1942-1952.
37. O'Hayre M, Salanga CL, Handel TM, Allen SJ. Chemokines and cancer: migration, intracellular signalling and intercellular communication in the microenvironment. *Biochem J*. 2008;409:635-649.
38. Laheij AM, de Soet JJ, Veerman EC, Bolscher JG, van Loveren C. The influence of oral bacteria on epithelial cell migration in vitro. *Mediators Inflamm*. 2013;2013:154532.
39. Haverman TM, Laheij A, de Soet JJ, de Lange J, Rozema FR. *Candida* and *Porphyromonas gingivalis*: the effect on wound closure in vitro. *J Oral Microbiol*. 2017;9:1328266.
40. Kotteas EA, Boulas P, Gkiozos I, Tsagkouli S, Tsoukalas G, Syrigos KN. The intercellular cell adhesion molecule-1 (icam-1) in lung cancer: implications for disease progression and prognosis. *Anticancer Res*. 2014;34:4665-4672.
41. Benedicto A, Herrero A, Romayor I, et al. Liver sinusoidal endothelial cell ICAM-1 mediated tumor/endothelial crosstalk drives the development of liver metastasis by initiating inflammatory and angiogenic responses. *Sci Rep*. 2019;9:13111.
42. Läubli H, Borsig L. Altered cell adhesion and glycosylation promote cancer immune suppression and metastasis. *Front Immunol*. 2019;10:2120.
43. Rho SS, Ando K, Fukuhara S. Dynamic regulation of vascular permeability by vascular endothelial cadherin-mediated endothelial cell-cell junctions. *J Nippon Med Sch*. 2017;84:148-159.
44. Golovkine G, Faudry E, Bouillot S, Voulhoux R, Attrée I, Huber P. VE-cadherin cleavage by LasB protease from Pseudomonas aeruginosa facilitates type III secretion system toxicity in endothelial cells. *PLoS Pathog*. 2014;10:e1003939.
45. Sukumaran SK, Prasadarao NV. Escherichia coli K1 invasion increases human brain microvascular endothelial cell monolayer permeability by disassembling vascular-endothelial cadherins at tight junctions. *J Infect Dis*. 2003;188:1295-1309.
46. Yang YM, Kim SY, Seki E. Inflammation and liver cancer: molecular mechanisms and therapeutic targets. *Semin Liver Dis*. 2019;39:26-42.
47. Suarez-Carmona M, Lesage J, Cataldo D, Gilles C. EMT and inflammation: inseparable actors of cancer progression. *Mol Oncol*. 2017;11:805-823.
48. Li L, Yu R, Cai T, et al. Effects of immune cells and cytokines on inflammation and immunosuppression in the tumor microenvironment. *Int Immunopharmacol*. 2020;88:106939.
49. Kikuchi H, Maishi N, Annan DA, et al. Chemotherapy-induced IL8 upregulates MDR1/ABCB1 in tumor blood vessels and results in unfavorable outcome. *Cancer Res*. 2020;80:2996-3008.
50. Grivennikov SI, Karin M. Dangerous liaisons: STAT3 and NF-kappaB collaboration and crosstalk in cancer. *Cytokine Growth Factor Rev*. 2010;21:11-19.
51. Greten FR, Grivennikov SI. Inflammation and cancer: triggers, mechanisms, and consequences. *Immunity*. 2019;51:27-41.
52. Sánchez-Alcoholado L, Ordóñez R, Otero A, et al. Gut microbiota-mediated inflammation and gut permeability in patients with obesity and colorectal cancer. *Int J Mol Sci*. 2020;21:6782.
53. Cani PD, Jordan BF. Gut microbiota-mediated inflammation in obesity: a link with gastrointestinal cancer. *Nat Rev Gastroenterol Hepatol*. 2018;15:671-682.
54. Bertocchi A, Carloni S, Ravenda PS, et al. Gut vascular barrier impairment leads to intestinal bacteria dissemination and colorectal cancer metastasis to liver. *Cancer Cell*. 2021;39:708-724.e711.
55. Nejman D, Livyatan I, Fuks G, et al. The human tumor microbiome is composed of tumor type-specific intracellular bacteria. *Science*. 2020;368:973-980.
56. Soutome S, Yanamoto S, Funahara M, et al. Preventive effect on post-operative pneumonia of Oral health care among patients who undergo esophageal resection: a multi-center retrospective study. *Surg Infect (Larchmt)*. 2016;17:479-484.
57. Jia C, Sun M, Wang W, Li C, Li X, Zhang X. Effect of oral plaque control on postoperative pneumonia following lung cancer surgery. *Thorac Cancer*. 2020;11:1655-1660.
58. Ishikawa S, Yamamori I, Takamori S, et al. Evaluation of effects of perioperative oral care intervention on hospitalization stay and postoperative infection in patients undergoing lung cancer intervention. *Support Care Cancer*. 2021;29:135-143.

SUPPORTING INFORMATION

Additional supporting information can be found online in the Supporting Information section at the end of this article.

How to cite this article: Yu L, Maishi N, Akahori E, et al. The oral bacterium *Streptococcus mutans* promotes tumor metastasis by inducing vascular inflammation. *Cancer Sci*. 2022;00:1-15. doi: 10.1111/cas.15538